

Experiments on the Structure of Turbulent CO/H₂/N₂ Jet Flames

R. S. Barlow
Combustion Research Facility
Sandia National Laboratories
Livermore, CA 94551-0969

G. J. Fiechtner and C. D. Carter
Innovative Scientific Solutions, Inc.
Dayton, OH 45440-3638

J.-Y. Chen
Department of Mechanical Engineering
University of California
Berkeley, CA 49720

Presented at the 1998 Spring Meeting of the
Western States Section/The Combustion Institute
Sandia National Laboratories, Berkeley, CA, March 23-24, 1998



Sandia National Laboratories

EXPERIMENTS ON THE STRUCTURE OF TURBULENT CO/H₂/N₂ JET FLAMES

R. S. BARLOW
*Combustion Research Facility
Sandia National Laboratories
Livermore, CA 94551-0969
barlow@ca.sandia.gov*

G. J. FIECHTNER, C. D. CARTER
*Innovative Scientific Solutions, Inc.
Dayton, OH 45440-3638*

and

J.-Y. CHEN
*Mechanical Engineering Department
University of California
Berkeley, CA 94720*

ABSTRACT

Scalar and velocity measurements are reported for two turbulent jet flames of CO/H₂/N₂. Simultaneous measurements of temperature, the major species, OH, and NO are obtained using the combination of Rayleigh scattering, Raman scattering, and laser-induced fluorescence. The two flames have the same jet Reynolds number of 16,700 but different nozzle diameters (4.58 mm and 7.72 mm). Axial profiles of velocity, mixture fraction, and major species mole fractions for these flames are in close agreement when streamwise distance is scaled by nozzle diameter. However, OH mole fractions are lower and NO mole fractions are higher near the stoichiometric flame length in the larger flame, due to longer residence times. Turbulent flame measurements are compared with steady strained laminar flame calculations. Laminar calculations show remarkably close agreement with measured conditional means of the major species when all diffusivities are set equal to the thermal diffusivity. In contrast, laminar flame calculations that include the normal treatment of molecular transport are clearly inconsistent with the measurements. These results suggest that turbulent transport is dominant over molecular diffusion in determining compositional structure at the locations considered in the present experiments, which begin at an axial distance of 20 nozzle diameters. Analysis of the conditional statistics of the differential diffusion parameter, $z = F_H - F_C$, supports this conclusion. With regard to validation of turbulent combustion models, this data set provides a target that retains the geometric simplicity of the unpiloted jet flame in coflow, while including a chemical kinetic system of intermediate complexity between hydrogen flames and the simplest hydrocarbon flames.

Note: This draft was generated for the WSS/CI S98 meeting. The literature review, references, and some sections of the discussion are not complete. We expect to submit a journal version in the near future. Please contact R. Barlow if you would like a preprint.

INTRODUCTION

Detailed scalar and velocity data sets are essential for the process of validating computational models for turbulent nonpremixed combustion. Laser diagnostics can provide nonintrusive measurements of the instantaneous velocities and species concentrations, and statistical information from such measurements may be used to evaluate a variety of modeling approaches. Despite the very productive history of laser diagnostics in combustion, the number of data sets available in the literature that are appropriate for the quantitative evaluation fundamental aspects of turbulent combustion models is relatively small. It is important for such data sets to include well-defined boundary conditions and relatively simple geometric configurations. It is also important that both velocity and scalar measurements be available for the same flame. Multi-component velocity measurements are preferable, as are multi-scalar measurements that include minor species. Minor species, such as combustion intermediates, radicals, and pollutants, tend to be sensitive to the details of interactions between fluid dynamics and chemical kinetics. Consequently, these species can provide information on the fundamental nature of these interactions, and the predictions of these minor species along with velocity, temperature, and major species constitutes a useful test for combustion models.

There are at least three detailed scalar and velocity data sets on hydrogen jet flames [1-4], and model calculation of some of these flames have been compared [5-7]. The present work focuses on jet flames of $\text{CO}/\text{H}_2/\text{N}_2$, which add a modest increment in chemical kinetic complexity, while retaining the simple geometry of the hydrogen jet flames. Raman/Rayleigh/LIF measurements were obtained at Sandia. Subsequently, through the collaborative framework of the International Workshop on Measurement and Computation of Turbulent Nonpremixed Flames [4], the velocity measurements were undertaken at ETH Zurich, Switzerland, and those experiments will be reported separately [8]. This paper focuses on the scalar measurements and includes only limited velocity data. Discussion of the scalar results emphasizes the issue of the relative importance of turbulent transport and differential molecular diffusion in these jet flames.

EXPERIMENTAL METHODS

Multiscalar experiments were conducted in the Turbulent Diffusion Flame (TDF) laboratory at Sandia. The flow facility, diagnostic systems, and calibration procedures have been described previously [9,10]. The combination of spontaneous Raman scattering and Rayleigh scattering was used to measure the major species concentrations and temperature. Linear laser-induced fluorescence (LIF) was used to measure the concentrations of OH and NO. Fluorescence signals were corrected on a shot-to-shot basis for variations in the Boltzmann fraction and collisional quenching rate, based on measured temperature and major species concentrations in the probe volume. Collisional quenching cross sections were based on the work of Paul et al. [11,12].

The precision of the scalar measurements is represented Fig. 1, which shows results of processed data from a series of CO/H_2 -air flat flames (50/50 fuel mixture) operated on a Hencken burner [9]. The symbols show mean temperature and species mole fractions from each operating condition of the burner, and each symbol is surrounded by an ellipse having major and minor axes of twice the standard deviation ($\pm\sigma$) of the scalar and the mixture fraction. The standard deviations in these calibrations may be used to estimate the contribution of random error (primarily shot noise) to the conditional fluctuations reported below. Representative values for precision measured at specific conditions are listed in Table 1. Estimates of systematic uncertainties (absolute accuracy of averaged values) are also listed in Table 1 and are based on analysis of the calibration methods, repeatability of calibrations, considerations of calibration drift, and allowances for uncertainties in the interpolated calibration curves for CO and H_2 . The accuracies of averaged temperature and concentration measurements are illustrated in Fig. 2. Here absolute concentrations are plotted versus the equivalence ratio for 18 flame conditions. The lower values from Table 1 are plotted as error bars. Where no error bars are visible the uncertainty is represented approximately by the size of the plotting symbol. The solid curves in Fig. 2 show results of non-adiabatic equilibrium calculations computed at temperatures representing the average Rayleigh temperature from several calibration sets. These averaged Rayleigh temperatures are about 50K below adiabatic.

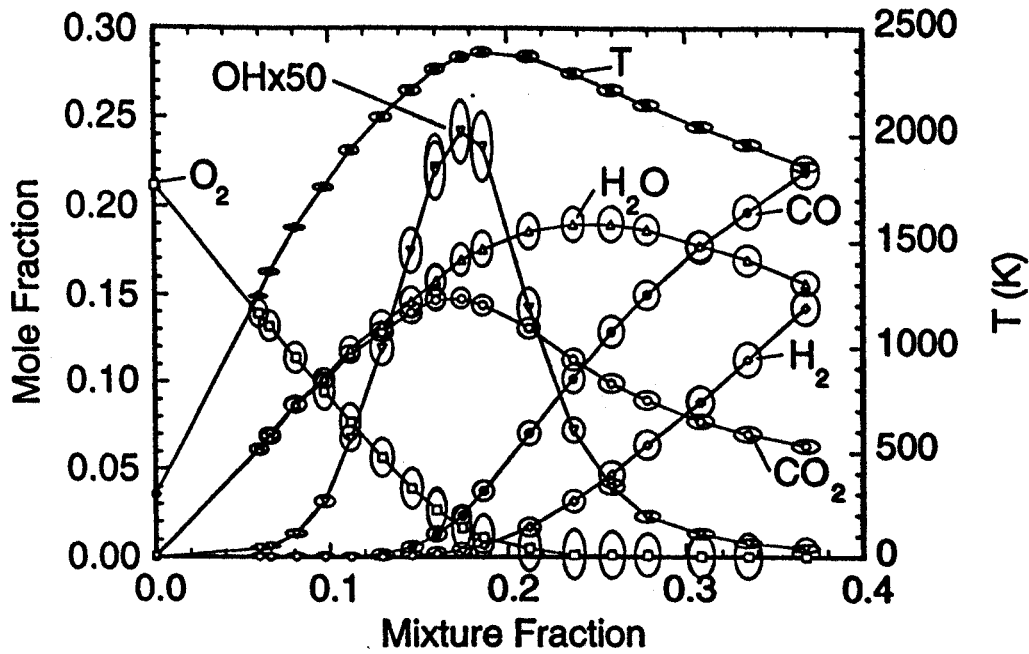


Fig. 1. Measured temperature and species mole fractions in the product gases above a series of CO/H₂-air calibration flames on the Hencken burner. Symbols show mean values from the Raman/Rayleigh/LIF data reduction process. Ellipses show standard deviations ($\pm\sigma$) of the measured scalars and the calculated mixture fraction.

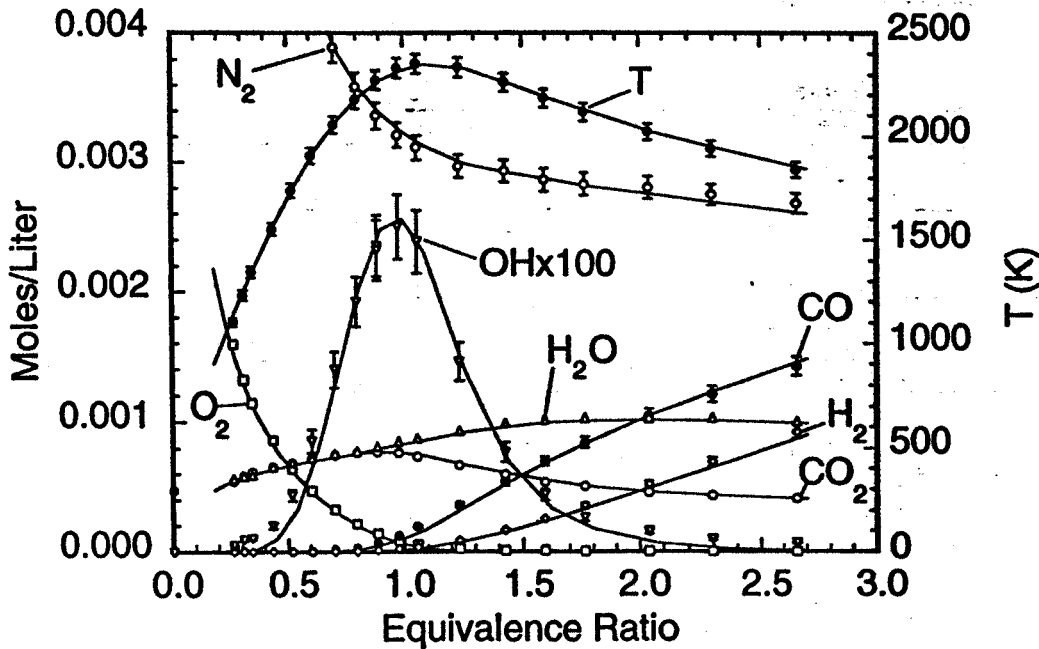


Fig. 2. Processed mean values of temperature and concentration in the CO/H₂-air Hencken flames. Error bars show estimated uncertainties, as listed in Table 1. Solid lines connect non-adiabatic equilibrium values calculated at the measured Rayleigh temperatures. The OH calibration is based on independent laser absorption measurements in a CH₄-air flame, and this is consistent with the calculated non-adiabatic equilibrium OH levels in the CO/H₂-air flames.

Table 1 Relative standard deviations of scalars measured in flat flames and estimated systematic uncertainties

Scalar	$\sigma(\text{rms})$	Conditions (mass fraction, T)	Systematic Uncertainty
T	1%	2140 K ^a	2%
Y _{N2}	2%	0.73, 2140 K ^a	3%
Y _{H2O}	5%	0.12, 2140 K ^a	3-5%
Y _{CO2}	6%	0.14, 2140 K ^a	3-5%
Y _{CO}	13%	0.062, 2020 K ^b	5-10%
Y _{H2}	17%	0.003, 2020 K ^b	5-10%
Y _{OH}	8%	0.0016, 2140 K ^a	10%
Y _{NO}	10%	8 ppm, 1760 K ^c	10-15%

- ^a Premixed CH₄/air, $\phi=0.96$, uncooled (Hencken) burner
- ^b Premixed CH₄/air, $\phi=1.27$, uncooled (Hencken) burner
- ^c Premixed CH₄/O₂/N₂, $\phi=0.72$, cooled (McKenna) burner

RESULTS AND DISCUSSION

Experiments were conducted on two jet flames with different nozzle diameters but equal Reynolds numbers based on the cold jet exit conditions. Nozzle dimensions and jet flow conditions are listed in Table 2. The nozzles were constructed from straight tubing with squared-off ends. The thick wall of the tubing provided a small recirculation zone that helped to stabilize the flames without a pilot. The fuel composition was 40% CO, 30% H₂, 30% N₂ by volume (syngas), and the flames were unconfined. Both flames appeared to be fully attached to the nozzle, and there is no evidence in the data that oxygen is entrained into the fuel jet through extinguished zones near the nozzle. The co-flow air conditions were 0.75 m/s \pm 0.05 m/s velocity, 290 K temperature, and 0.012 mole fraction of H₂O vapor.

Table 2 Nozzle Dimensions and Flow Conditions^{*}

Flame	d, Nozzle ID (mm)	Nozzle OD (mm)	U _{jet} (m/s)	Re _{jet}
A	4.58	6.34	76.0 \pm 1.5	~16,700
B	7.72	9.46	45.0 \pm 0.9	~16,700

$$* \text{Re} = U_{\text{jet}} d / \nu, \text{ where } \nu = 2.083 \times 10^{-5} \text{ m}^2/\text{s}$$

Axial profiles were obtained in both flames and include measurements from $x/d=20$ to $x/d=75$ with steps of 5d. Radial profiles were obtained at axial positions of $x/d=20, 30, 40, 50,$ and 60 in each flame. Typically, 800 to 1000 shots were collected at each location in these profiles. The sections that follow report Favre- and conditionally averaged mole fractions of the measured scalars. The data base available on the web includes Favre, Reynolds, and conditional statistics of mass fractions, as well as mole fractions. In addition, the complete files of single-shot mass fractions and mole fractions are available.

Here and in the archived data files the mixture fraction is calculated from the data following the method of Bilger et al. [13].

$$F = \frac{2(Y_C - Y_{C,2})/w_C + (Y_H - Y_{H,2})/2w_H - (Y_O - Y_{O,2})/w_O}{2(Y_{C,1} - Y_{C,2})/w_C + (Y_{H,1} - Y_{H,2})/2w_H - (Y_{O,1} - Y_{O,2})/w_O},$$

where Y's are elemental mass fractions of carbon, hydrogen, and oxygen; w's are atomic weights; and the subscripts 1 and 2 refer to the fuel stream and co-flowing air stream, respectively. The fuel and air boundary conditions are listed in Table 3.

Table 3 Elemental Mass Fraction Boundary Conditions*

Stream	Y_C	Y_H	Y_O
Fuel, 1	0.2377	0.0299	0.3167
Coflow, 2	0.0	7.7×10^{-4}	0.2356

* Coflow humidity included, CO_2 content in air neglected, balance is N_2 .

Axial and Radial Profiles

Axial profiles of Favre averaged mixture fraction, temperature, and species mole fractions are plotted in Fig. 3 (left side) for the two flames, with the axial coordinate normalized by nozzle diameter. In these fully connected flames with low coflow velocity the scaling by nozzle diameter works well for all measured scalars except for the mole fractions of OH and NO. The OH and NO mole fractions are more strongly influenced by local scalar dissipation and by convective residence time than are temperature and the major species. Consequently, OH mole fractions are 20-25% lower in flame B than in flame A, and NO levels are about 40% higher. It is this greater sensitivity of the minor species to fluid-dynamic scaling that make them useful for the evaluation of turbulent combustion models. Axial profiles of scalar fluctuations are also plotted in Fig. 3 (right side). Again, the scaling of axial distance by nozzle diameter demonstrates the similarity of the two flames. Note also that the fluctuations in temperature and products H_2O and CO_2 pass through local minima at the streamwise locations where the corresponding mean values reach their peaks.

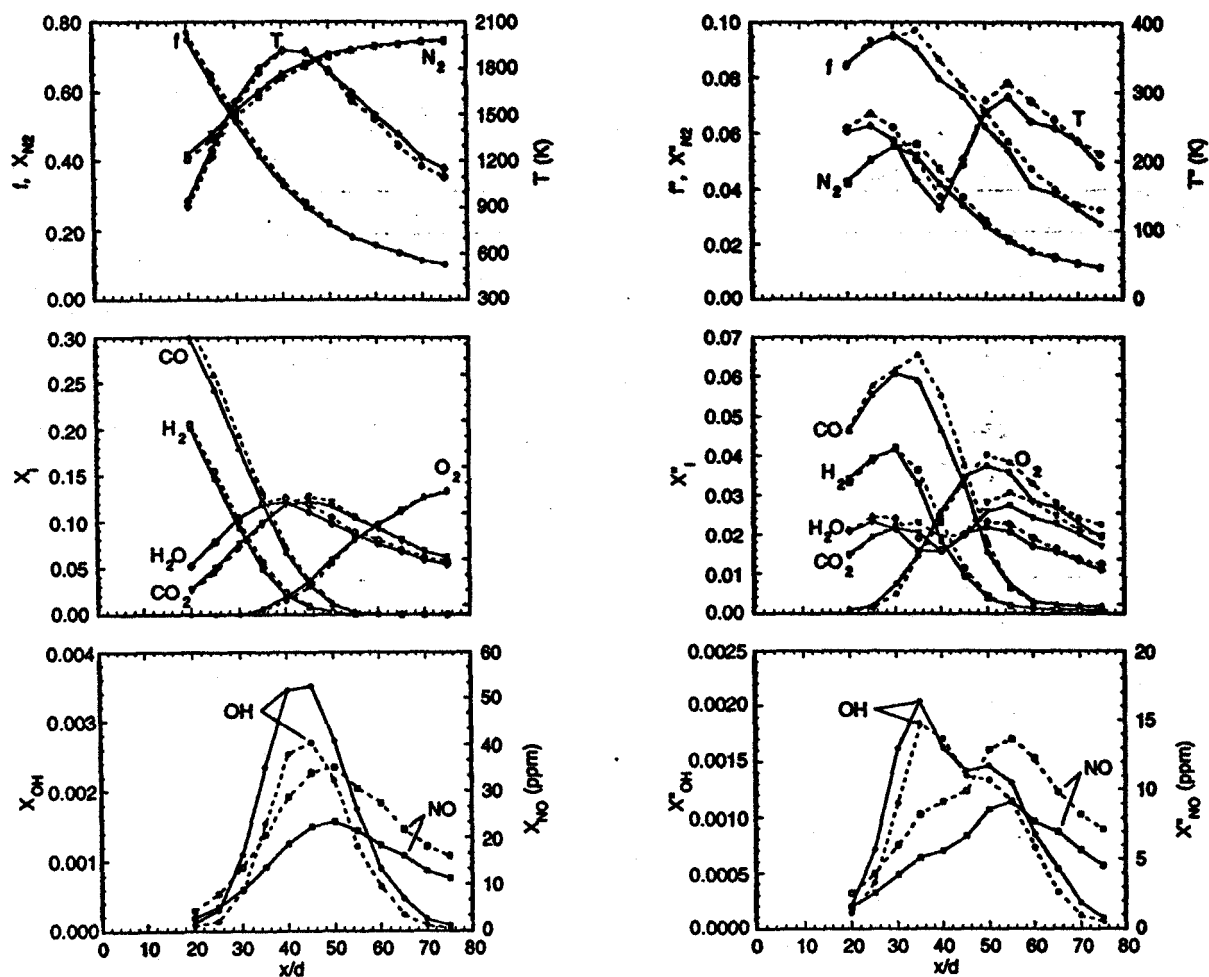


Fig. 3. Axial profiles of Favre averaged scalars (left side) and rms fluctuations (right side) for the two flames, A (solid lines) and B (dashed lines).

Radial profiles of Favre averaged scalars at streamwise locations of $x/d=20$ and $x/d=50$ are plotted in Fig. 4. Again the simple scaling by nozzle diameter works well for temperature and major species in these flames. However, OH levels are lower and NO levels are higher in flame B than in flame A, due to the longer residence times in the larger flame. Axial and radial profiles of the normalized mean and fluctuation of the streamwise component velocity, as reported by Flury [8], are shown in Figs. 5 and 6 to emphasize the availability of velocity measurements in these flames.

Axial and radial profiles of velocity and scalars provide an important first level of information on jet flame structure that may be used in the testing and evaluation of turbulent combustion models. However, such profiles yield little information on the details of the relationships among species and the influence of turbulence on scalar transport and reaction progress. Consequently, they are necessary but not sufficient for the establishment of a complete quantitative understanding of the capabilities and limitations of turbulent combustion models, nor are such profiles particularly useful for developing fundamental insights on the effects of turbulence-chemistry interactions. These issues may be better explored in mixture fraction space.

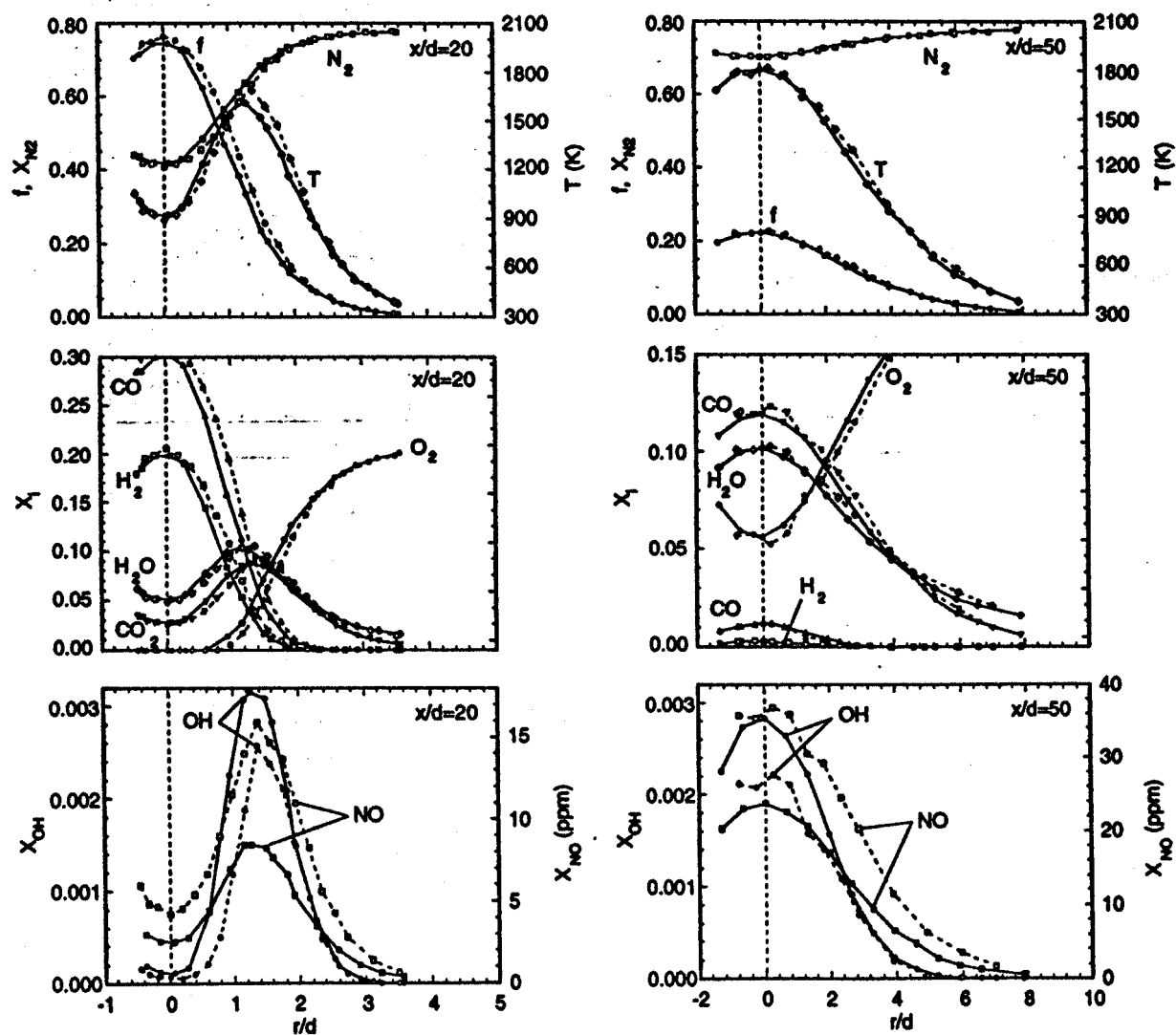


Fig. 4. Radial profiles of Favre averaged scalars in the two flames, A (solid lines) and B (dashed lines), measured at axial locations $x/d=20$ (left) and $x/d=50$ (right). The Favre average stoichiometric flame length is $\sim 47d$ in both flames.

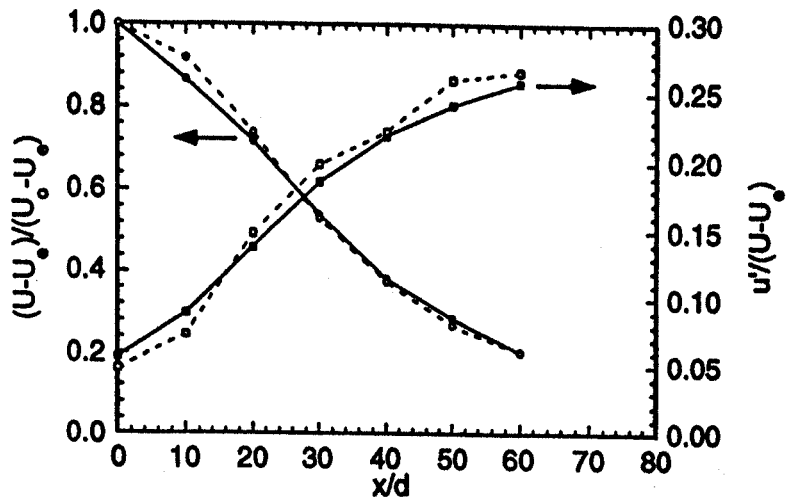


Fig. 5. Axial profiles of mean and fluctuating velocity from LDA measurements by Flury [8] for flames A (solid lines) and B (dashed lines). U_c is the coflow velocity. U_e is the nozzle exit velocity on the centerline.

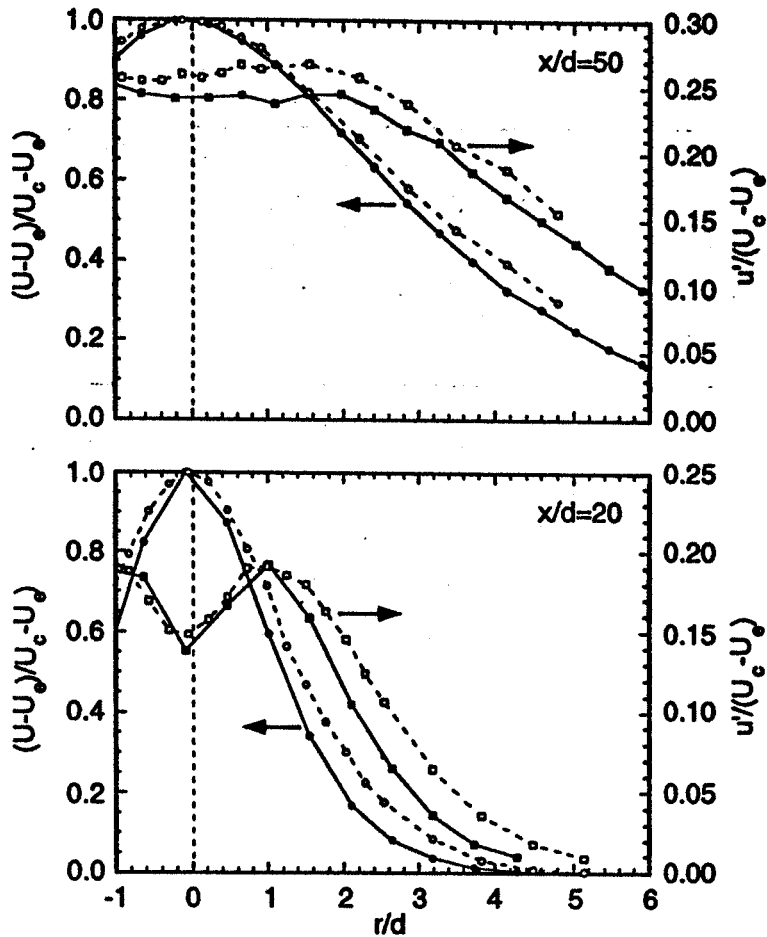


Fig. 6. Radial profiles of mean and fluctuating axial velocity from LDA measurements by Flury [8] for flames A (solid lines) and B (dashed lines) at $x/d=20$ (lower graph) and $x/d=50$ (upper graph). U_c is the coflow velocity. U_e is the nozzle exit velocity on the centerline.

Conditional Statistics and Issues of Scalar Transport

In the present flames there is no evidence of localized extinction at the measured locations nor of the entrainment of oxygen into the fuel jet through extinguished or lifted regions at the flame base. This is demonstrated in Fig. 7, which is a scatter plot of temperature and the mole fraction of O_2 . In these fully connected flames the scalar structure may be represented conveniently by the conditional mean and rms fluctuation, rather than the complete scatter plots or pdf's. As an illustration, Fig. 8 shows the conditional means of temperature and O_2 mole fraction corresponding to the scatter data in Fig. 7, with the conditional rms fluctuations ($\pm\sigma$) plotted as uncertainty bars.

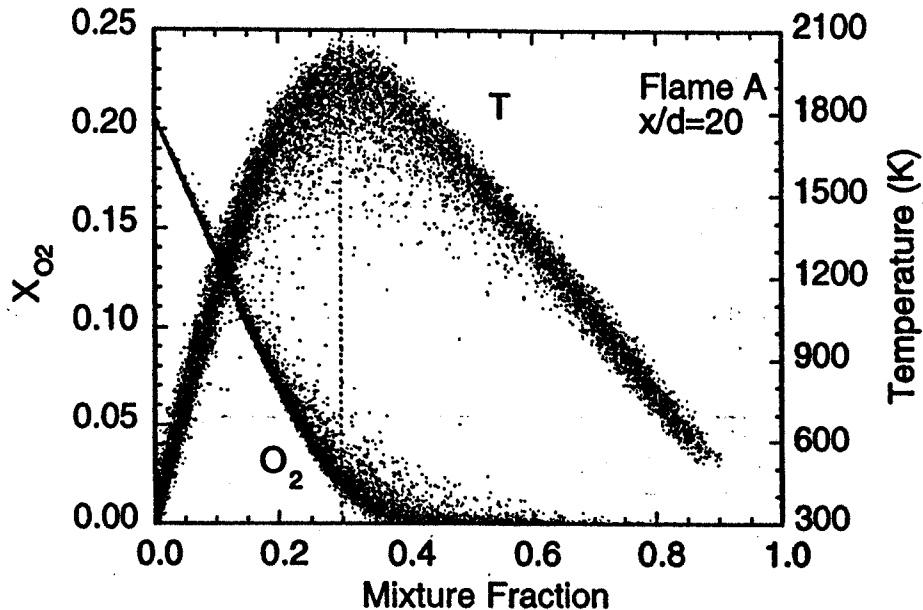


Fig. 7. Scatter plot of single-shot temperature and O_2 measurements in flame A at $x/d=20$, including approximately 15,000 samples from the complete radial profile. The vertical dashed line indicates the stoichiometric value of the mixture fraction.

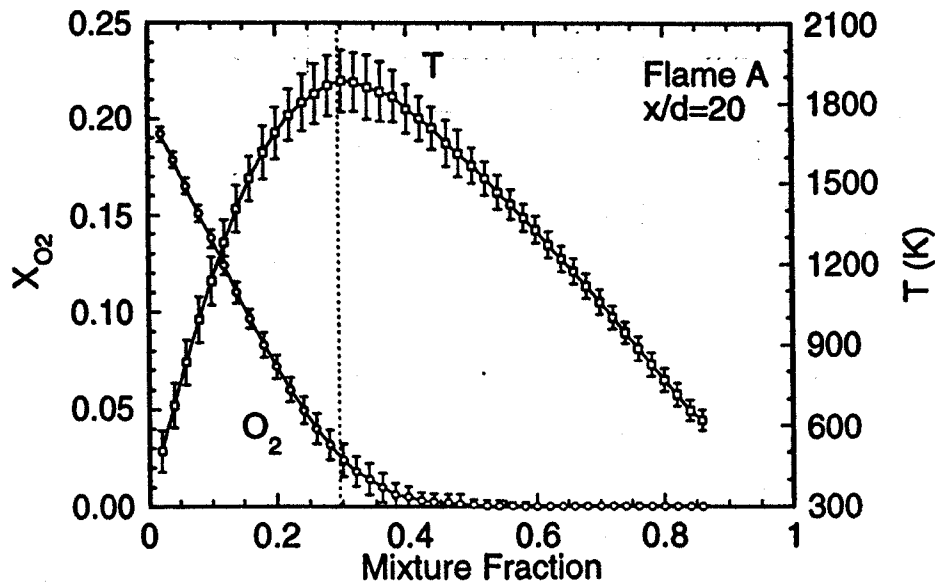


Fig. 8. Conditional mean and rms fluctuation (plotted as uncertainty bars) calculated from the data of Fig. 7, using evenly-spaced intervals of 0.02 in mixture fraction. The vertical dashed line indicates the stoichiometric value of the mixture fraction.

Scatter data and conditional means of scalars measured in turbulent flames have often been compared with results of steady strained opposed-flow laminar flame calculations. Initial comparisons for the present CO/H₂/N₂ flames revealed large differences between measurements and laminar calculations that included the normal Chemkin treatment of mass diffusion. Laminar calculations were repeated with all species diffusivities set equal to the thermal diffusivity, and results are shown in Fig. 9. Large differences are seen in the mole fractions of H₂, CO, H₂O, and CO₂. The most obvious effect is that the H₂O/CO₂ ratio decreases by a factor of two near the stoichiometric value of the mixture fraction, when equal diffusivities are prescribed. Figure 10 compares measurements from flame A at $x/d=30$ with the two types of laminar calculations, both with strain parameter of $a=100\text{ s}^{-1}$. The agreement between the equal-diffusivity calculation and the turbulent flame data is remarkable, suggesting that turbulent transport is dominant over molecular diffusion in determining major species mole fractions.

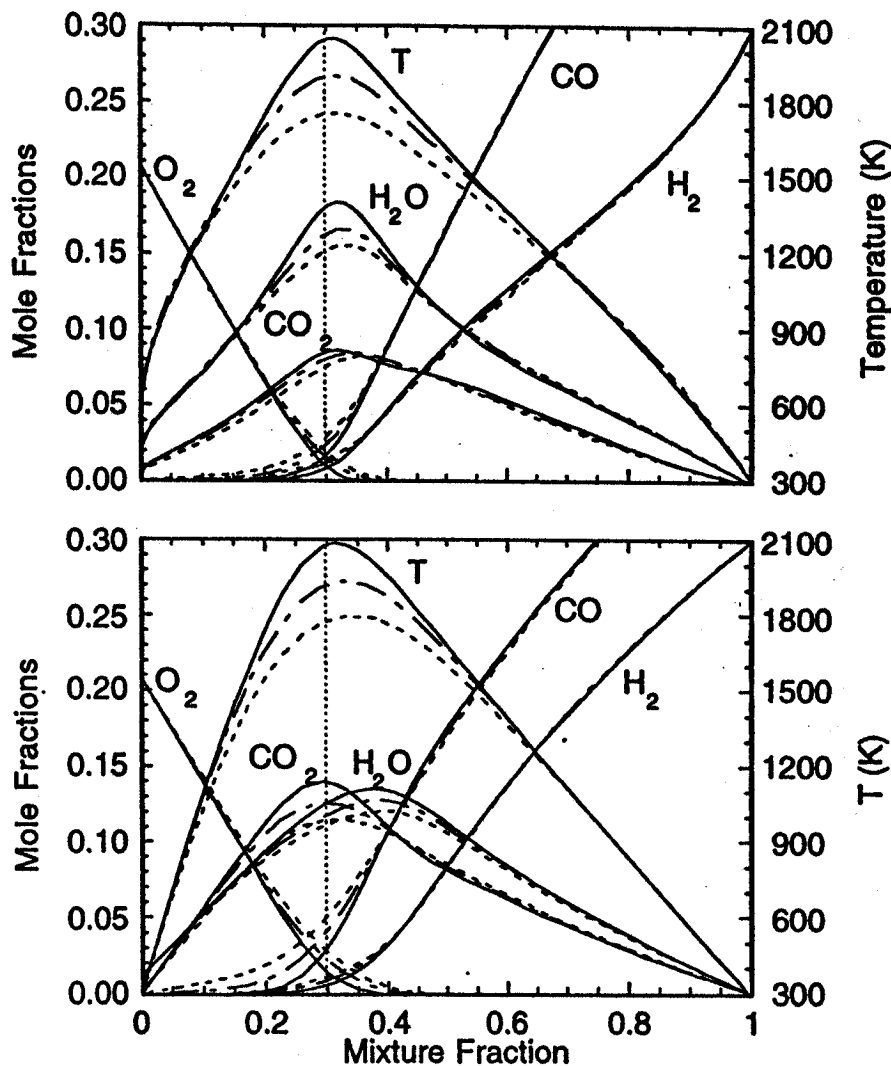


Fig. 9. Results of steady strained opposed-flow laminar flame calculations corresponding to the fuel and air boundary conditions of these turbulent jet flame experiments. Curves for three values of the strain parameter (Tsuiji geometry) are plotted in each graph, $a=10$ (solid), 100 (chain-dash), and 400 s^{-1} (dash). The results in the upper graph include full molecular transport (Chemkin), while the lower graph shows the effect of setting all species diffusivities equal to the thermal diffusivity. The vertical dashed line indicates the stoichiometric value of the mixture fraction.

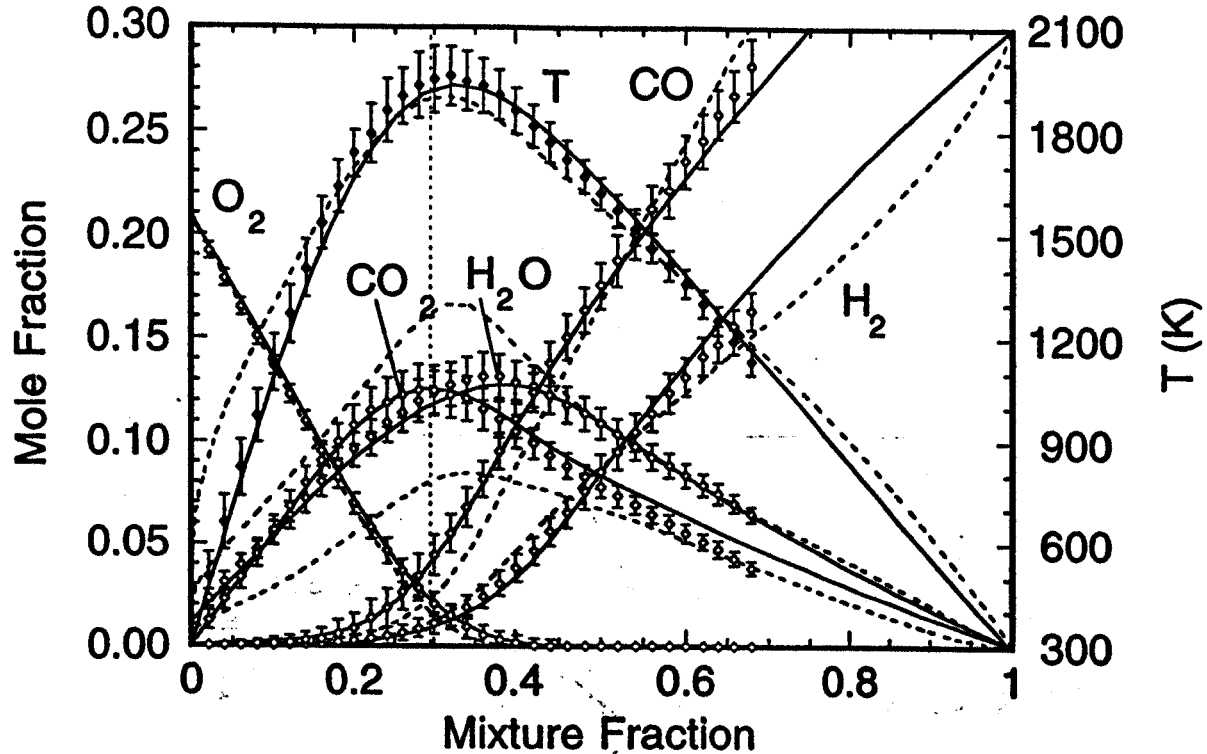


Fig. 10. Measured conditional means and rms fluctuations at $x/d=30$ in flame A compared with the two types of laminar calculations: full transport (dash lines) and equal diffusivities (solid lines). The vertical dashed line indicates the stoichiometric value of the mixture fraction.

Figure 11 shows the streamwise evolution of the conditional mean and rms fluctuation of temperature and major species in the two flames. Equal-diffusivity calculations are included in each plot with $a=10$ or 100 s⁻¹ depending on which result better approximates the local measurements. The data are consistent with the expected trend of decreasing strain and scalar dissipation rates with increasing streamwise distance. It is also clear that there are greater effects of finite rate chemistry in flame A than in flame B. There is some evidence of differential species diffusion in fuel-rich portions of the jet flames. In particular, the measured CO/H₂ ratio in fuel-rich mixtures is somewhat greater than indicated by the equal-diffusivity results.

The degree of differential diffusion may be quantified by defining and comparing elemental mixture fractions. Here, we define mixture fractions for hydrogen and carbon as:

$$F_H = \frac{Y_H - Y_{H,1}}{Y_{H,2} - Y_{H,1}} \quad \text{and} \quad F_C = \frac{Y_C - Y_{C,1}}{Y_{C,2} - Y_{C,1}}$$

A differential diffusion parameter, $z = F_H - F_C$, can then be calculated as the difference between elemental mixture fractions. Figure 12 shows calculated results for F_H , F_C , and z plotted versus the Bilger mixture fraction from steady laminar flame calculations using the conventional Chemkin molecular transport package. Preferential diffusion of H₂ toward the reaction zone causes a deficit in hydrogen relative to carbon in region $0.55 < F_{\text{Bilger}} < 1$, and there is a positive peak in z just on the rich side of the stoichiometric condition.

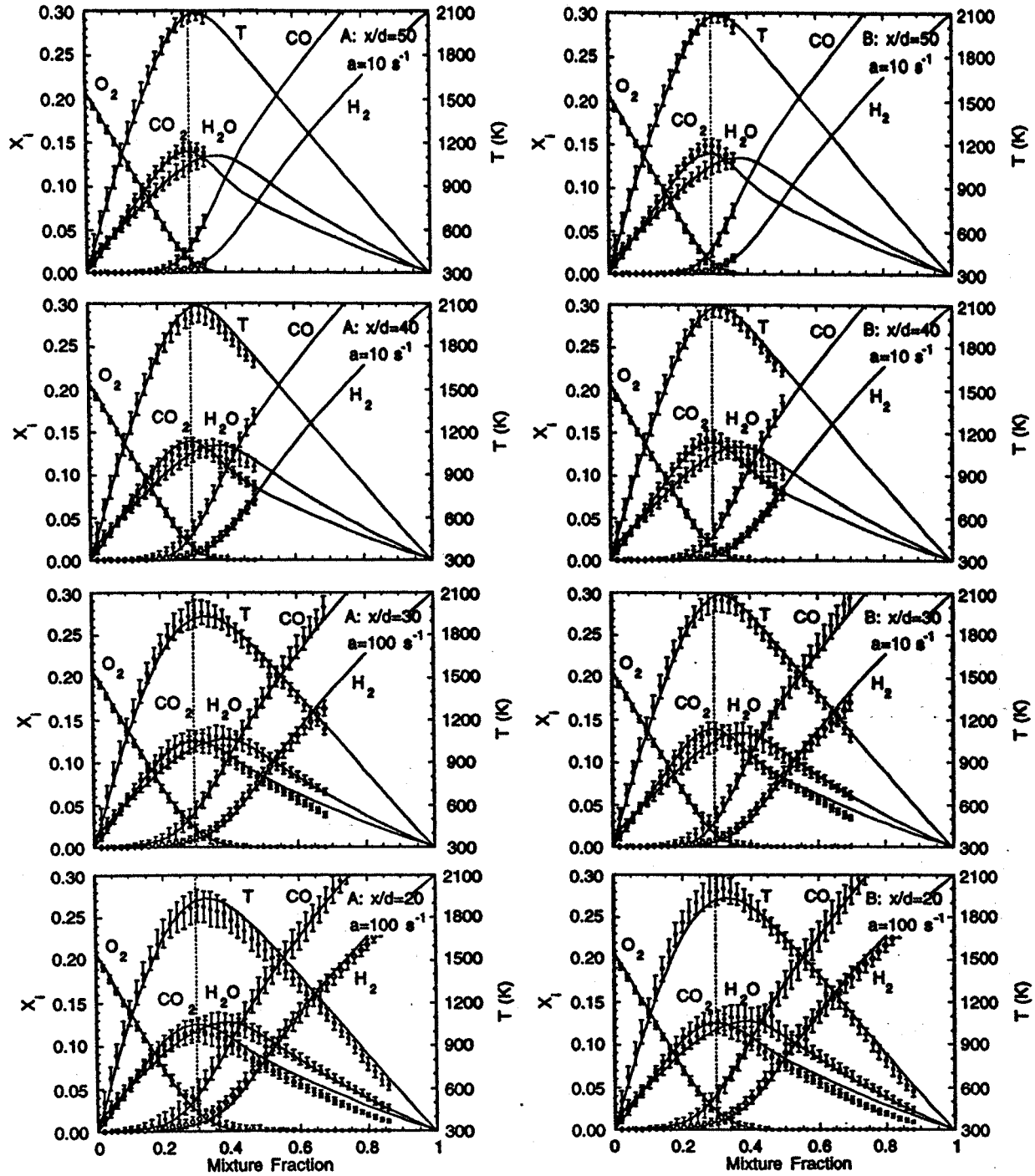


Fig. 11. Streamwise evolution of conditional statistics in the two jet flames. Solid curves show results of equal diffusivity laminar flame calculations at the strain rate indicated in each flame.

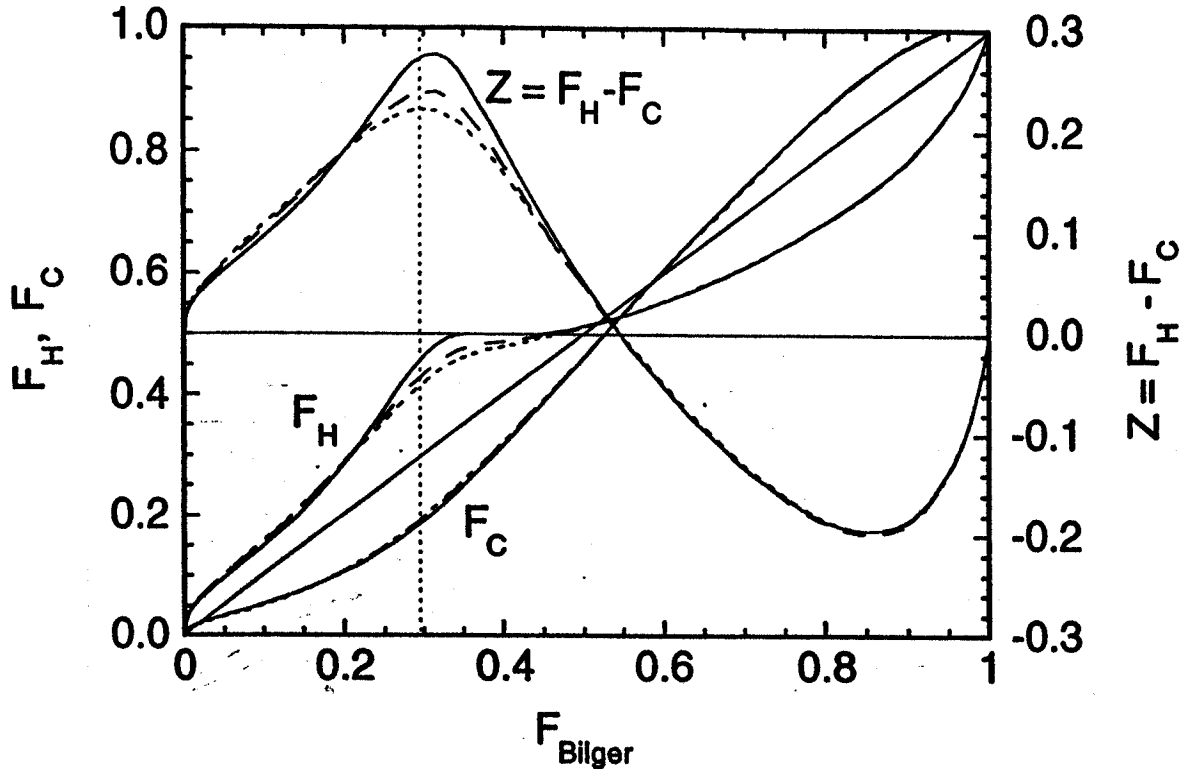


Fig. 12. Elemental mixture fractions F_H and F_C and the differential diffusion parameter z plotted versus the Bilger mixture fraction. Results are from the steady laminar flame calculations with full transport conducted at strain rates of $a=10$ (solid), 100 (chain-dash), and 400 s^{-1} (dash).

Figure 13 shows the streamwise evolution of F_H , F_C , and z in each of the two turbulent flames. Here the symbols show conditional means, and the conditional rms fluctuations are plotted as error bars ($\pm\sigma$). Several observations may be made. First, for the turbulent flame conditions and locations considered in these experiments the measured effects of differential diffusion are much smaller than in the laminar calculations. Second, the largest differential diffusion effects are observed in the richest samples at each streamwise location, such that the conditional mean z is close to zero for lean and near-stoichiometric samples, but tails off toward negative values at the fuel-rich end of each data set. This streamwise evolution of z is believed to reflect a mixing history that involves preferential diffusion of H_2 out of the core of the jet near the flame base, where heat release tends to laminarize the flow, particularly at lower Reynolds numbers. Once this initial deficit of hydrogen is created in the richest samples, it tends to be preserved far down stream because the richest samples at any streamwise location are those which have been least affected by turbulent stirring. A third observation is that the conditional fluctuations in z tend to decrease with downstream distance. In fact, the level of fluctuation at $x/d=50$ is comparable to the noise in measurements above a steady premixed flat flame, and any fluctuations in z that exist near the tips of these jet flames are too small to be measured accurately by the present diagnostics. We note that larger differential diffusion effects are likely to be present closer to the nozzle, as reported by Meier et al. [2] for nitrogen-diluted H_2 flames.

It is possible to subtract out the shot noise contribution to the conditional fluctuations of z , as done by Smith et al. [14]. This approximate procedure is based upon the reasonable assumption that random errors in z are statistically independent of the actual turbulent fluctuations. The noise contribution can then be derived from the rms fluctuations of z obtained from the flat-flame calibration data. We have not applied this procedure for the present version of this paper.

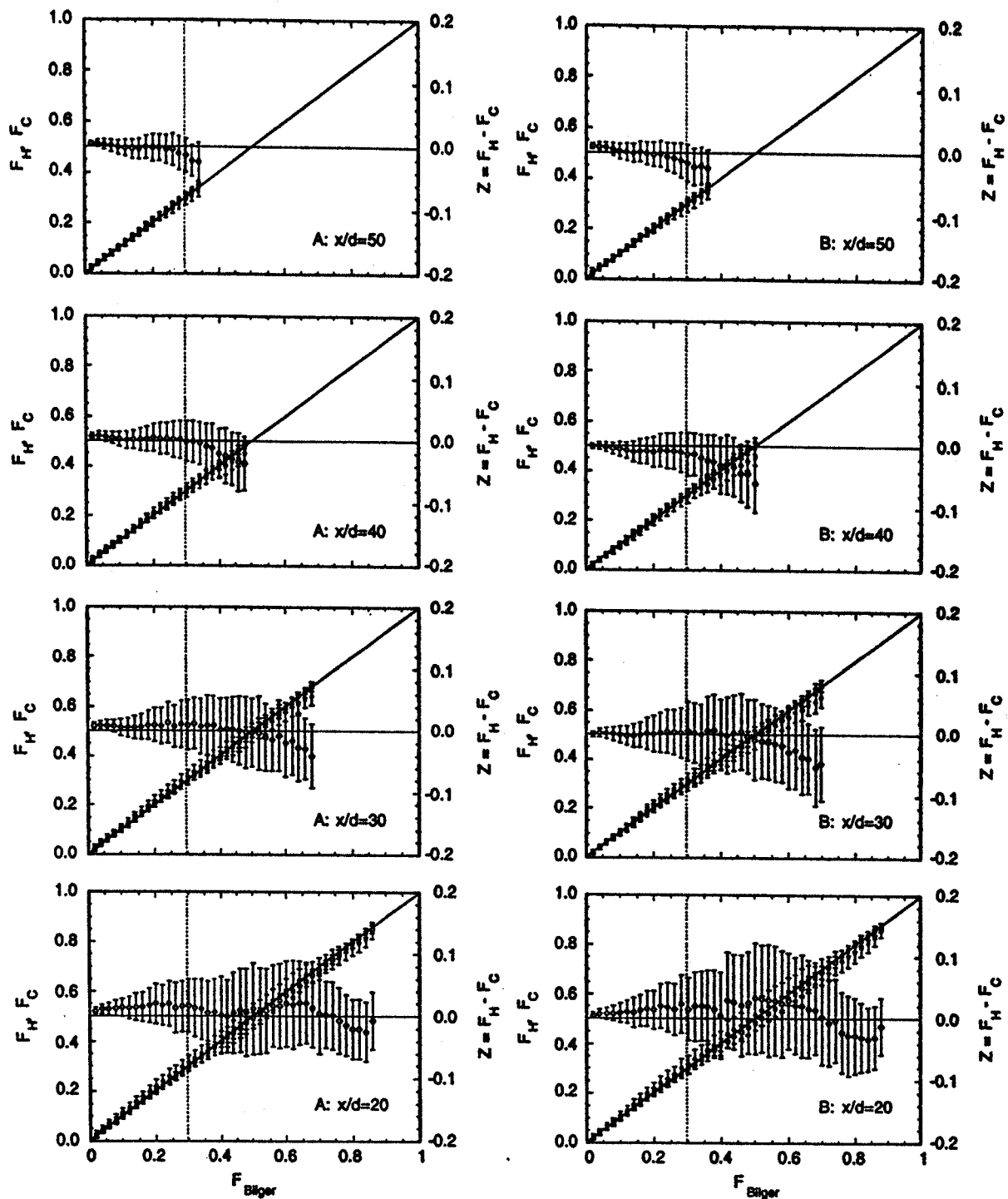


Fig. 12. Streamwise evolution of F_H (squares), F_C (circles), and z (diamonds) in flames A and B. Note expanded scale for z .

CONCLUSIONS

The scalar measurements presented here, combined with the corresponding three-component velocity measurements of Flury, constitute a relatively complete data set on piloted jet flames of $\text{CO}/\text{H}_2/\text{N}_2$. These geometrically simple flames represent a modest increment in complexity over hydrogen jet flames, with regard to the process of systematic evaluation of

turbulent combustion models. Results presented here have focused on the relative importance of turbulent transport versus molecular diffusion in determining conditional statistics of major species concentrations. Comparisons with two types of laminar flame calculations have shown that the turbulent flame results are better approximated by laminar flame calculations that prescribe equal diffusivities. This indicates that turbulent mixing is dominant over molecular diffusion in determining major species mole fractions at the locations measured in the present experiments. Analysis of elemental mixture fractions of hydrogen and carbon and of the differential diffusion parameter z , defined as the difference between these elemental mixture fractions, has confirmed that differential diffusion effects in the turbulent flames are small compared to those in laminar flames computed using full molecular transport.

Acknowledgments

Work at Sandia was supported by the United States Department of Energy, Office of Basic Energy Sciences. CDC was supported by the AFOSR under Air Force Contract F33615-92-2202.

REFERENCES

1. Barlow, R. S., and Carter, C. D., *Combust. Flame* 97:261-280 (1994); and *Combust. Flame* 104:288-299 (1996).
2. Meier, W., Vydorov, A. O., Bergmann, V., and Stricker, W., *Appl. Phys. B* 63:79-90 (1996).
3. Neuber, A., Krieger, G., Tacke, M., Hassel, E. P., and Janicka, J., *Combust. Flame* 113:198-211 (1998).
4. Data archives of the International Workshop on Measurement and Computation of Turbulent Nonpremixed Flames, www.ca.sandia.gov/tdf/Workshop.html.
5. Chen, J.-Y., Chang, Y.-C., and Koszykowski, M., *Comb. Sci. Tech.* 110:505 (1996).
6. Barlow, R. S., Smith, N. S. A., Chen, J.-Y., and Bilger, R. W., "Nitric Oxide Formation in Dilute Hydrogen Jet Flames: Isolation of the Effects of Radiation and Turbulence-Chemistry Submodels," *Combust. Flame*, accepted (1998)
7. Schlatter, M., Ferreira, J. C., Flury, M. and Gass, J., *Twenty-Sixth Symposium (International) on Combustion*, The Combustion Institute, Pittsburgh, PA, 1996, pp. 2215-2222.
8. Flury, M., Ph.D. thesis and paper in preparation, ETH Zurich, Switzerland.
9. Nguyen, Q. V., Dibble, R. W., Carter, C. D., Fiechtner, G. J., and Barlow, R. S., *Combust. Flame* 105:499-510 (1996).
10. Barlow, R. S., Fiechtner, G. J., and Chen, J.-Y., *Twenty-Sixth Symposium (International) on Combustion*, The Combustion Institute, Pittsburgh, PA, 1996, pp. 2199-2205.
11. Paul, P. H., *JQSRT* 51:511-524 (1994).
12. Paul, P. H., Gray, J. A., Durant Jr., J. L., and Thoman Jr., J. W., *AIAA J.* 32:1670-1675 (1994).
13. Bilger, R. W., Stårner, S. H., and Kee, R. J., *Combust. Flame* 80:135-149 (1990).
14. Smith, L. L., Dibble, R. W., Talbot, L., Barlow, R. S., and Carter, C. D., *Combust. Flame* 100:153-160 (1995).